Optics Letters

Direct laser writing structural color for reversible encryption and decryption in different mediums

Bin Dong,[1] Bingrui Liu,[1,4] Chao Chen,[2] Dawei Wang,[1] Leran Zhang,[1] Liqun Xu,[1] Wei Xiong,[3] Jiawen Li,[1] Yanlei Hu,[1] Jiaru Chu,[1] and Dong Wu[1,*]

[1]CAS Key Laboratory of Mechanical Behavior and Design of Materials, Department of Precision Machinery and Precision Instrumentation, University of Science and Technology of China, Hefei, Anhui 230027, China
[2]School of Materials Science and Engineering, Hefei University of Technology, Hefei 230009, China
[3]Wuhan National Laboratory for Optoelectronics, Huazhong University of Science and Technology, Wuhan, China
[4]brliu@ustc.edu.cn
*dongwu@ustc.edu.cn

Received 3 February 2023; revised 17 March 2023; accepted 21 March 2023; posted 5 April 2023; published 4 May 2023

Structural color (SC) has enormous potential for improving the visualization and identification of functional micro/nano structures for information encryption and intelligent sensing. Nevertheless, achieving the direct writing of SCs at the micro/nano scale and the change of color in response to external stimuli simultaneously is rather challenging. To this end, we directly printed woodpile structures (WSs) utilizing femtosecond laser two-photon polymerization (fs-TPP), which demonstrated obvious SCs under an optical microscope. After that, we achieved the change of SCs by transferring WSs between different mediums. Furthermore, the influence of laser power, structural parameters, and mediums on the SCs was systematically investigated, and the mechanism of SCs using the finite-difference time-domain (FDTD) method was further explored. Finally, we realized the reversible encryption and decryption of certain information. This finding holds broad application prospects in smart sensing, anti-counterfeiting tags, and advanced photonic devices. © 2023 Optica Publishing Group

https://doi.org/10.1364/OL.486950

Color exists in nature in two forms, known as chemical color and physical color. Chemical color is produced based on pigment's selective absorption of light with certain wavelength. Physical color is also known as structural color (SC) and is attributed to the refraction, diffuse reflection, diffraction or interference of periodic micro/nano structures. Compared with chemical color, which will fade with the gradual oxidation of pigment when exposed, the persistence of SCs is directly related to the integrity of the micro/nano structures. In the meantime, the development of intelligent micro/nano actuators makes it possible to achieve the change of SCs in response to external stimuli (magnetic field, mediums [1], pH [2], voltage [3,4], stress [5], optical field [6], etc.), which is rarely seen with chemical color. For instance, a blood sugar sensor was developed based on the change of SCs in response to the concentration of glucose [7]. In addition to these, Lai *et al*. achieved a stress sensor by self-assembling one layer of close-packed polystyrene nanoparticles on the surface of a polydimethylsiloxane (PDMS) substrate [8].

The above-mentioned stimuli-responsive application of SCs lies within macroscopic scenarios. However, the patterning of SCs at a macroscale usually requires the assistance of certain templates, and only one color can be produced at each time. The fabrication of macroscopic SCs based on surface plasmon resonance (SPR) usually involves techniques such as electron beam evaporation, chemical deposition, and other post-processing methods [9,10], which are too complex and inefficient. Nevertheless, SCs fabricated by self-assembly [11,12] suffer from low resolution due to the lack of control techniques in the manufacturing. In contrast, the fabrication of SCs at a microscale can significantly improve the display resolution and information density, and the color can be adjusted by tuning the manufacturing parameters accordingly. At the same time, the processing of microscopic SCs requires precision manufacturing techniques, such as direct laser writing (DLW) [13]. As opposed to the above-mentioned methods, DLW has much higher degree of processing freedom. DLW can easily achieve processing precision of the order of sub-microns [14–17] in combination with femtosecond laser two-photon polymerization (fs-TPP), which endows DLW with higher display resolution and broad application prospects in high-resolution imaging. Femtosecond DLW (fs-DLW) stimuli-responsive periodic micro/nano structures have been employed to fabricate four-dimensional (4D) photonic structures. For example, a 4D-printed colorimetric microscopic sensor was realized based on the material's intrinsic response to temperature and humidity [18]. In the meantime, the concealing of SC patterns under stress and revealing under heating has been achieved through fs-DLW shape memory polymers (SMPs) [19]. However, the encryption and decryption of SC patterns in response to the change of surrounding chemical mediums is still demanding but has rarely been reported.

Herein, we utilized state-of-the-art fs-DLW technology to fabricate woodpile structures (WSs) with commercially available photoresist SZ2080—which exhibits different expansion ratios in various mediums—and achieved significant SCs. Firstly, we systematically investigated the influence of structural parameters on the coloration of WSs. Later, we explored the mechanism of the emergence of SCs based on the finite-difference time-domain

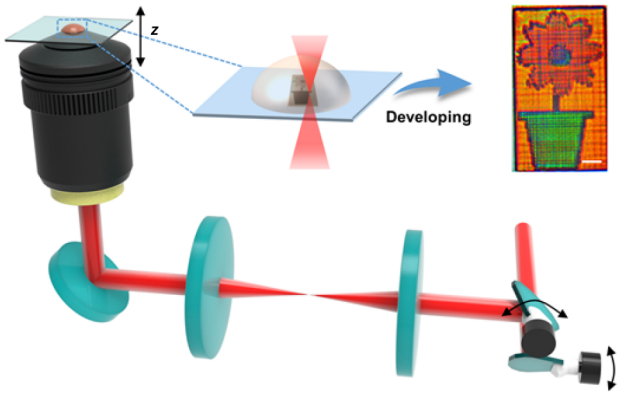

Fig. 1. Schematic of the fs-TPP processing system. In the top right corner lie the magnified view of fs-DLW SCs and optical micrograph of the flower pattern after development. The scale bar represents 10 μm.

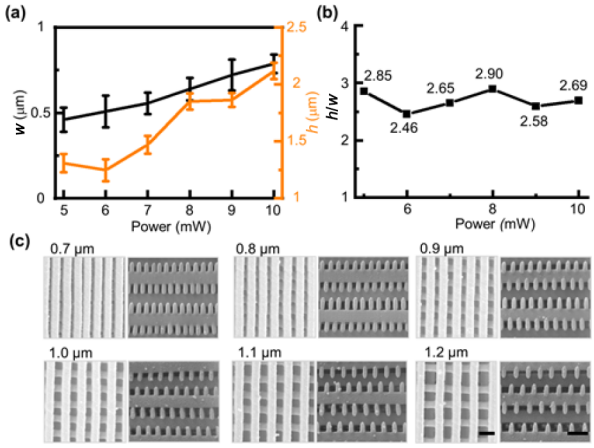

Fig. 2. Characterization of fs-TPP and fabrication of WSs. (a) is the influence of laser power on the linewidth w and height h, (b) is the influence of laser power on the h/w ratio, and (c) is the demonstration of the top and side SEM images of WSs with a_{xy} ranging from 0.7 μm to 1.2 μm with a step of 100 nm, and a_z as 1.0 μm. Scale bars represent 1 μm (left) and 2 μm (right).

(FDTD) method. According to the transmittance spectra and simulation results, the change of SCs should mainly be attributed to the change of interference and the overall decrease of transmittance because of the contraction of WSs. Finally, we designed patterns based on WSs and realized reversible encryption and decryption of certain information in different chemical mediums.

In this paper, *in situ* fabrication of WSs with different structural parameters was achieved by an fs-TPP system, which is shown in Fig. 1. The Galvo scanning system is mainly composed of two Galvo mirrors, whose scanning directions are perpendicular to each other. In this way, the focal point of the fs laser can move freely in the xy plane. Combined with the movement of a linear stage along the z axis, this processing system can actually fabricate arbitrary 3D micro/nano structures with extremely high precision. This paper proposes an fs-DLW WS for its simplicity, fast manufacturing speed, and excellent mechanical stability. The magnified schematic diagram of the fabricated pattern and the pattern after development is shown in the top right corner of Fig. 1. The detailed structural parameters and shown in Fig. S1 in Supplement 1. The WS is composed of a series of orthogonal lines, as shown in Fig. S2 in Supplement 1. Every four layers make up a period. The lines between the first two layers are mutually perpendicular to each other, and the other two layers have a half line-spacing bias compared to the first two. a_{xy} and a_z represent the line spacing and layer spacing of WSs, respectively, while w and h represent the width and height of each line, respectively.

In order to facilitate the further fabrication of WSs with SZ2080, we studied the influence of laser power on the processing precision of the photoresist by writing lines between two blocks. The composition of SZ2080 [20] is shown in Fig. S3 in Supplement 1. With the increasing of laser power, the linewidth w and line height h increase simultaneously, but the height–width ratio h/w remains ~2.5, as shown in Figs. 2(a) and 2(b), respectively. Figure 2(c) demonstrates the scanning electron microscope (SEM) images of the top and side view of the WSs. When a_{xy} is 0.7 μm, the spacing between lines is very small. Although theoretically two lines won't merge when a_{xy} is less than 0.7 μm, the spacing is so small that the lines are extremely hard to separate in development. When a_z is larger than 1.2 μm, the layer spacing is larger than the height of lines, so that the separation of two layers might occur, which is detrimental to the holistic stability of the WSs. After that, the influence of structural parameters, for instance, a_{xy} and a_z, and laser power, as well as surrounding mediums on the SCs, was systematically investigated, as shown in Fig. S4 in Supplement 1. Figures S4(a), S4(b), and S4(c) in Supplement 1 are the transmittance optical micrographs of WSs with laser power of 6, 8, and 10 mW in ethanol, air, and deionized (DI) water, respectively. All the optical micrographs are obtained under a 5× objective lens. The writing speed was set as 200 μm/s if not specified. It's worth noting that almost all WSs turned black in air and DI water when the laser power was fixed at 6 mW, which can be utilized for the encryption of SC patterns. At the same time, the colors of WSs with same structural parameters in air and DI water showed little difference because of the hydrophobicity of SZ2080. DI water can't permeate into the micro/nano pores of WSs, so the expansion ratios in air and DI water are rather similar, which will soon be discussed in detail. Meanwhile, the influence of ethanol concentration on the SCs is shown in Fig. S5 in Supplement 1. We take a_{xy} as 0.8 μm and a_z as 1.0 μm as an example. When the concentration of ethanol reached 20%, the SCs showed a sudden change, indicating that ethanol had permeated into the micro/nano pores of the WSs, thus leading to the overall expansion.

Photoresist SZ2080 could expand [21] in some specific solvents, which is directly related to the affinity between structure and solvent, the degree of crosslinking, and other inherent properties of the material. The lower the degree of crosslink, or the higher the affinity, the greater the expansion ratio. To characterize the expansion of the structure in different mediums, a four-layer WS was placed upon a pillar, and its deformation in ethanol, air, and DI water was recorded under an optical microscope, as illustrated in Fig. 3(a). The spatial dimensions of the WS adopted were $40 \times 40 \times 4$ μm^3. According to the experimental results in Fig. 3(b), the affinity between structure and solvent demonstrated significant influence on the expansion ratio. In organic solvents, such as ethanol, n-propyl alcohol, or acetone, the fine structure can be fully permeated, so the expansion ratio was estimated at around 5%. In air, the size of the structure is

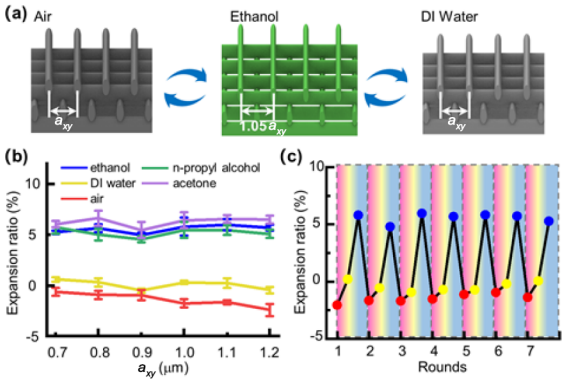

Fig. 3. Characterization of the expansion of SZ2080 in different mediums. (a) is the schematic diagram of the expansion of WSs in ethanol, air, and DI water, (b) is the extracted expansion ratio of WSs in ethanol, n-propyl alcohol, acetone, DI water, and air, respectively, and (c) is the cyclic test of expansion ratio by transferring WS with a_{xy} as 1.0 μm and a_z as 1.0 μm to air (red dot), DI water (yellow dot), and ethanol (blue dot), in order.

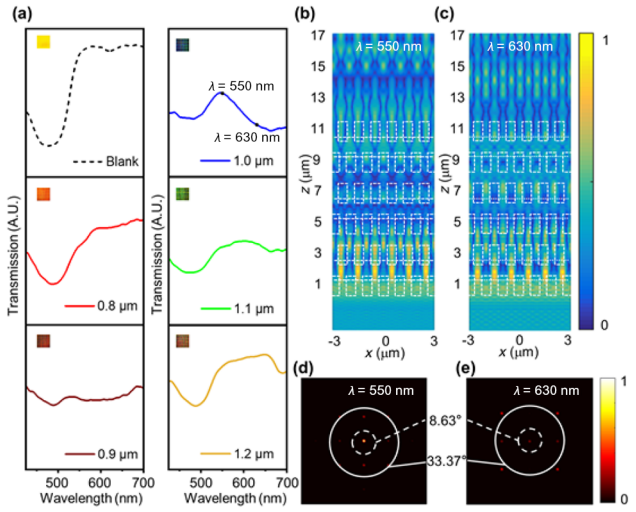

Fig. 4. FDTD simulation over the emergence of SCs. (a) is the experimental transmittance spectra of WSs with a_{xy} ranging from 0.8 μm to 1.2 μm with a step of 100 nm, and a_z as 1.0 μm. The experimental transmittance spectra were collected under a 50× objective lens. (b) and (c) are the sectional electric field amplitude distributions acquired using the FDTD method at wavelengths of 550 nm and 630 nm, respectively. (d) and (e) are the normalized far-field electric field distributions acquired using the FDTD method at wavelengths of 550 nm and 630 nm, respectively. The white circles represent the collection angle (CA) for the microscope used in this work (CA = 8.63° for a 5× objective lens, CA = 33.37° for a 50× objective lens). The simulation results in (b)–(e) were obtained with a_{xy} as 1.0 μm and a_z as 1.0 μm.

slightly smaller than the design size. However, for the solvent with low affinity to the structure, for instance DI water, it can hardly penetrate into the micro/nano pores, so the size of WS is almost the same as the design size. After that, we ran a cyclic test to verify the stability of the expansion of SZ2080 in different mediums. As we can see from Fig. 3(c), the expansion ratio of WSs demonstrates excellent consistency after transferring to air (red dot), DI water (yellow dot), and ethanol (blue dot) in order for multiple times.

To facilitate our understanding of the mechanism of SCs, especially its emergence and change, we acquired the transmittance spectra of WSs in ethanol, as shown in Fig. 4(a). We chose such wavelengths because SCs are only practical when they fall under the visible spectrum. The black dashed line represents the transmission spectrum of SZ2080 blocks. It's worth noting that the peaks of spectral curves demonstrate a certain degree of redshift with the increasing of a_{xy}. The corresponding optical micrographs are in the top left corner.

In the meantime, FDTD simulation was also carried out. When a beam of polychromatic light is injected from the bottom of a WS, the transmitted beams are diffracted by each layer. To illustrate our idea more clearly, we took a WS with a_{xy} of 1.0 μm and a_z of 1.0 μm as an example. Figure S6 in Supplement 1 shows the comparison between experimental transmittance spectra and simulation results, which demonstrates great congruence. Figures 4(b) and 4(c) show the sectional electric field amplitude distributions at a wavelength of 550 nm and 630 nm, respectively. The wavelengths of 550 nm and 630 nm correspond to the marked peak and dip of the spectrum, respectively, as marked in Fig. 4(a). Figures 4(d) and 4(e) are the normalized far-field electric field distribution at a wavelength of 550 nm and 630 nm, respectively. Compared with the wavelength at 630 nm, the energy of wavelength at 550 nm is more concentrated in the zeroth order, whereas the diffraction of wavelength at 630 nm is more obvious with energy dispersed in the (0, 0), (0, ± 1), (±1, 0), and (±1, ± 1) orders, some of which won't be collected by the objective lens.

As an example, we acquired the transmittance spectra with a_{xy} as 1.0 μm (left) and 1.1 μm (right), and a_z as 1.0 μm in DI water in Fig. S7 in Supplement 1 and compared them with that in ethanol. The overall transmittance of WSs in DI water decreased significantly compared to that in ethanol. Because of the overall contraction of WSs leading to the increase of line spacing, less light will propagate through WSs, so an overall drop of transmittance was observed. At the same time, because of the decrease of structural parameters in DI water, the diffraction patterns of WSs will also change. However, the transmittance spectra were obtained under a 50× objective lens [collection angle (CA) = 33.37°]. As we all know, higher orders of diffraction tend to possess less energy, which means that the objective lens can always collect most transmitted light and the difference caused by the change of diffraction patterns is almost negligible, so that the positions of transmission peak showed little shift. From the perspective of SCs, the contraction of WSs only results in the change of color brightness and the color chromaticity remains unchanged so we can conclude that, besides the change of interference, the decrease of overall transmittance is also an important factor involving in the change of SCs in different mediums.

The premise of SCs being able to be put into practical applications is the ability to maintain stability when switching between different mediums. Here we tested the stability of SZ2080 SCs by running cyclic tests. In Fig. 5(a), we can see that the recovered spectrum overlapped pretty well with the original spectrum after a round of transferring between ethanol, air, and DI water. After that, we chose a_{xy} as 1.1 μm and a_z as 1.0 μm to run multiple rounds of transferring. According to Fig. 5(b), it's apparent that the SCs maintained excellent stability considering that the spectral curves basically overlapped and the SCs didn't show much obvious change.

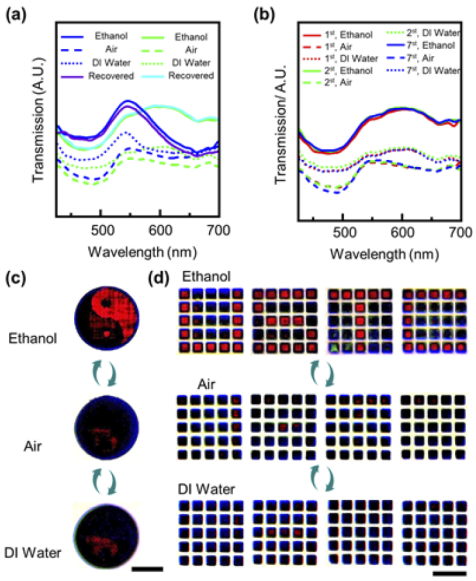

Fig. 5. Cyclic tests and demonstration of SCs. (a) is one round of cyclic test with a_{xy} as 1.0 μm (blue and purple line) and 1.1 μm (green and cyan line), and a_z as 1.0 μm, (b) is multiple rounds of cyclic test with a_{xy} as 1.1 μm and a_z as 1.0 μm, and (c) and (d) are the Taichi diagram and letters achieved by fs-DLW and their color changing in ethanol, air, and DI water, respectively. The laser power was fixed at 6 mW. The scale bars represent 40 μm in (c) and 50 μm in (d).

WSs with different structural parameters can be freely positioned and concatenated to enable SC printing of two-dimensional (2D) images. Typically, there are two ways to achieve the patterning of SCs. The first is to program in MATLAB to match the structural parameters with the numerical values and positions of pixels. The advantage of such an approach is its flexibility and versatility, so that the patterning of any picture is tangible. The disadvantages are also obvious, for example the defect around the edges of different SC components due to the discontinuity of structural parameters. The second method is to fabricate arrays of SC cubes, each of which represents a pixel. This method is suitable for regular and simple images, for example numbers and letters. We have successfully fabricated the Taichi diagram and letters (U, S, T, C) employing the above-mentioned techniques, as shown in Figs. 5(c) and 5(d), respectively.

In Fig. 5(c), a_{xy} was set as 0.8 μm (orange) and 1.1 μm (black), respectively, and a_z was set as 1.0 μm. The laser power was preset as 6 mW if not specified. In ethanol, the contrast between two colors in the Taichi diagram was markedly intense. However, once transferred to the air, the transmittance decreased due to the overall contraction of WSs, so the SCs with different parameters tended to be similar, such that information encryption was achieved. After that, WSs were transferred into DI water. Due to the hydrophobicity of photoresist SZ2080, the feature size of WSs was roughly unchanged, so the patterns remained hidden. Similarly, in Fig. 5(d), a_{xy} was set as 0.8 μm (orange) and 1.0 μm (black), respectively, and a_z was set as 1.0 μm. The size of each pixel was 13×13 μm^2, and the spacing between pixels was 7 μm. The contrast between two colors of the letters was obvious enough to identify the information in ethanol, but the letters could be encrypted once transferred to air or DI water.

In conclusion, we successfully fabricated micro/nano WSs with obvious SCs and realized the encryption and decryption of specific patterns utilizing the different expansion ratios of photoresist SZ2080 in different mediums. Besides these, we collected the transmittance spectra of WSs and explored the mechanism of color changing using FDTD simulation. The above-mentioned work has enormous potential application in high-density information encryption and anti-counterfeiting tags.

Acknowledgment. The authors acknowledge the Experimental Center of Engineering and Material Sciences at USTC for the fabrication and measurement of samples. This work was partly carried out at the USTC Center for Micro and Nanoscale Research and Fabrication.

Disclosures. The authors declare no conflicts of interest.

Data availability. Data underlying the results presented in this paper are not publicly available at this time but may be obtained from the authors upon reasonable request.

Supplemental document. See Supplement 1 for supporting content.

REFERENCES

1. J. H. Kim, G. H. Lee, J. B. Kim, and S. H. Kim, Adv. Funct. Mater. **30**, 2001318 (2020).
2. B. Liu, B. Dong, C. Xin, C. Chen, L. Zhang, D. Wang, Y. Hu, J. Li, L. Zhang, and D. Wu, Small **19**, 2204630 (2023).
3. W. Zhang, H. Li, and A. Y. Elezzabi, Adv. Funct. Mater. **32**, 2108341 (2022).
4. D. Franklin, Y. Chen, A. Vazquez-Guardado, S. Modak, J. Boroumand, D. Xu, S.-T. Wu, and D. Chanda, Nat. Commun. **6**, 7337 (2015).
5. M. L. Tseng, J. Yang, M. Semmlinger, C. Zhang, P. Nordlander, and N. J. Halas, Nano Lett. **17**, 6034 (2017).
6. L. Qin, X. Liu, K. He, G. Yu, H. Yuan, M. Xu, F. Li, and Y. Yu, Nat. Commun. **12**, 699 (2021).
7. D. Nakayama, Y. Takeoka, M. Watanabe, and K. Kataoka, Angew. Chem. **115**, 4329 (2003).
8. X. Lai, J. Peng, Q. Cheng, A. P. Tomsia, G. Zhao, L. Liu, G. Zou, Y. Song, L. Jiang, and M. Li, Angew. Chem. **133**, 14428 (2021).
9. X. Duan and N. Liu, ACS Nano **12**, 8817 (2018).
10. X. Duan, S. Kamin, and N. Liu, Nat. Commun. **8**, 14606 (2017).
11. H. K. Raut, H. Wang, Q. Ruan, H. Wang, J. G. Fernandez, and J. K. Yang, Nano Lett. **21**, 8602 (2021).
12. Y. Ohtsuka, M. Sakai, T. Seki, R. Ohnuki, S. Yoshioka, and Y. Takeoka, ACS Appl. Mater. Interfaces **12**, 54127 (2020).
13. J. Huang, L. Jiang, X. Li, A. Wang, Z. Wang, Q. Wang, J. Hu, L. Qu, T. Cui, and Y. Lu, Nanophotonics **8**, 869 (2019).
14. V. Mizeikis, V. Purlys, R. Buividas, and S. Juodkazis, J. Laser Micro Nanoen **9**, 42 (2014).
15. Y. Liu, H. Wang, J. Ho, R. C. Ng, R. J. Ng, V. H. Hall-Chen, E. H. Koay, Z. Dong, H. Liu, and C.-W. Qiu, Nat. Commun. **10**, 4340 (2019).
16. H. Liu, H. Wang, H. Wang, J. Deng, Q. Ruan, W. Zhang, O. A. Abdelraouf, N. S. S. Ang, Z. Dong, and J. K. Yang, ACS Nano **16**, 8244 (2022).
17. X. Cao, Y. Du, Y. Guo, G. Hu, M. Zhang, L. Wang, J. Zhou, Q. Gao, P. Fischer, and J. Wang, Adv. Mater. **34**, 2109161 (2022).
18. M. Del Pozo, C. Delaney, C. W. Bastiaansen, D. Diamond, A. P. Schenning, and L. Florea, ACS Nano **14**, 9832 (2020).
19. W. Zhang, H. Wang, H. Wang, J. Y. E. Chan, H. Liu, B. Zhang, Y.-F. Zhang, K. Agarwal, X. Yang, and A. S. Ranganath, Nat. Commun. **12**, 112 (2021).
20. A. Ovsianikov, J. Viertl, B. Chichkov, M. Oubaha, B. MacCraith, I. Sakellari, A. Giakoumaki, D. Gray, M. Vamvakaki, and M. Farsari, ACS Nano **2**, 2257 (2008).
21. S. Rekštytė, D. Paipulas, M. Malinauskas, and V. Mizeikis, Nanotechnology **28**, 124001 (2017).